ISSN 1693-9220 (Print) | 2987-8713 (Online), Volume 20, No. 2 (2026), pp. 144-156

International Journal of Enterprise Modelling

Published by: International Enterprise Integration Association

Empirical characterization of test platform effects on single-axis CubeSat reaction wheel ADCS with IoT-based PID tuning

Bayu Nuar Khadapi Hasibuan[1], Dananjaya Ariateja[2], Satriya Utama[3], Rangga Taqwa[4], Ria Aprilianingsih[5]

[1,2,4,5]Department of Electrical Engineering, Faculty of Defense Engineering and Technology, Republic of Indonesia Defense University, Bogor, Indonesia

[3] National Research and Innovation Agency, Satellite Technology Research Center Rancabungur, Bogor, Indonesia

Abstract

Terrestrial testing of CubeSat Attitude Determination and Control System (ADCS) prototypes presents fundamental validation challenges because no laboratory platform perfectly replicates the free-floating microgravity condition of orbit. The empirical effect of such platform-induced dynamics on closed-loop reaction-wheel control performance, particularly for low-cost academic CubeSat programs, remains insufficiently characterized. This study aims to empirically compare two widely used low-cost test platforms a string suspension and a free bearing for a single-axis reaction-wheel ADCS prototype and to quantify how each platform's parasitic dynamics constrain PID controller performance. A 1.5U CubeSat-class prototype with an ESP32-based controller, BNO055 IMU, and a Blynk Cloud IoT interface for real-time PID tuning was tested over five sessions (>1 hour of cumulative active testing). Performance was quantified using the Time-in-±5° metric, error standard deviation, settling time, and number of direction reversals. Quantitative results show that the string suspension yields a peak Time-in-±5° of 8.8% with error standard deviation of ±90.7–119.9°, driven by torsional-pendulum dynamics, while the free bearing yields a peak Time-in-±5° of only 1.2% with a stuck-and-jump signature characteristic of stiction. A Karnopp-friction simulation in Python reproduces a permanent steady-state error of ~5° under stiction, quantitatively validating stiction as the dominant non-linearity. The novelty of this work lies in the integrated combination of empirical multi-platform characterization, Karnopp-based stiction validation, and an open-source IoT-based PID tuning framework within a single low-cost experimental system, providing actionable guidance for academic CubeSat ADCS development under limited-facility conditions.

Corresponding Author:

Bayu Nuar Khadapi Hasibuan,
Department of Electrical Engineering, Faculty of Defense Engineering and Technology
Republic of Indonesia Defense University,
Kawasan IPSC Sentul, Jl. Anyar, Sukahati, Kec. Citeureup, Kabupaten Bogor, Jawa Barat 16810, Indonesia,
bayuhasibuan405@gmail.com.

Article Info

Article history:

Received : May 09, 2026
Revised : May 19, 2026
Accepted : May 21, 2026

Keywords:

Attitude Control;
CubeSat;
IoT;
PID Controller;
Reaction Wheel;
Stiction.

Introduction

CubeSats have emerged as a transformative platform in modern space missions due to their low cost, fast development cycles, and standardized form factor. As of 2024, more than 2,000 CubeSats have

been launched globally, with applications ranging from Earth observation, scientific research, space weather monitoring, to constellation-based communication networks (Liddle et al., 2020).
The Attitude Determination and Control System (ADCS) is one of the most critical subsystems in a CubeSat, responsible for orienting the spacecraft to point its payload, antennas, or solar panels with the required precision (Khan et al., 2022; Wertz, 1978)

Among various ADCS actuators, the reaction wheel is widely used due to its ability to provide precise, smooth, and repeatable torque without requiring external mass expulsion (Sidi, 1997). The principle of operation is based on the conservation of angular momentum: by accelerating an internal flywheel, the reaction wheel applies an equal and opposite torque on the spacecraft body. This makes reaction wheels well-suited for fine attitude maneuvers required for nadir pointing, sun tracking, and inertial pointing modes (Carrara, 2014a; Ismail & Varatharajoo, 2010a)

Despite the maturity of reaction wheel technology in larger spacecraft, its implementation in CubeSat-class platforms presents several engineering challenges (Xia et al., 2017a). CubeSats have very limited mass and volume budgets, which constrain the size and inertia of the reaction wheel relative to the satellite body. Furthermore, the development of ADCS algorithms requires extensive testing on ground-based platforms before flight qualification (Krogstad & Gravdahl, 2008). However, no terrestrial platform perfectly replicates the free-floating microgravity condition of orbit. Common test platforms such as air bearings, magnetic levitation, and string suspensions each introduce their own dynamics that may not exist in space (Schwartz et al., 2003).

This issue is particularly acute for low-cost academic CubeSat development programs that often rely on simple test platforms due to budget and infrastructure constraints (Modenini et al., 2020a). While extensive literature exists on reaction wheel design and ADCS algorithms (Ismail & Varatharajoo, 2010; Ovchinnikov et al., 2018), comparatively little attention has been paid to the empirical characterization of how different test platform configurations affect the validation of ADCS controllers, especially in undergraduate and academic research contexts (Dief et al., 2023) .

This paper addresses this gap by presenting an empirical study of two test platform configurations for a single-axis reaction wheel ADCS prototype: a string suspension and a free bearing. The prototype is a 1.5U CubeSat-class platform controlled by an ESP32 microcontroller with a BNO055 inertial sensor and a BLDC motor with bidirectional Electronic Speed Controller (ESC) (Helmy et al., 2022). To enable rapid and reproducible PID tuning, an Internet of Things (IoT) interface based on Blynk Cloud is implemented, allowing wireless real-time parameter adjustment and data logging (Espinoza-Nunez & Roman-Gonzalez, 2022) .

This paper presents three main contributions: (1) an empirical analysis of the dynamic behavior of two test platform configurations using multiple PID parameter combinations; (2) the development of a Python-based stiction-aware simulation using the Karnopp friction model to validate stiction as the dominant non-linearity; and (3) an open-source IoT-based PID tuning framework utilizing Blynk Cloud for low-cost academic CubeSat research (Olsson et al., 1998a).The paper is organized into methodology, experimental results, discussion, and conclusion sections.

Despite the rich body of literature on reaction-wheel ADCS design and friction modeling, a specific research gap persists. Most existing studies either (i) evaluate ADCS algorithms on high-fidelity but expensive air-bearing testbeds available only in well-funded laboratories (Schwartz et al., 2003; Modenini et al., 2020a), or (ii) focus on simulation-only validation without confronting the parasitic dynamics of low-cost terrestrial platforms (Helmy et al., 2022.; Khan et al., 2022). The empirical question of how non-ideal platform effects—particularly torsional-pendulum dynamics on string suspensions and stiction on free bearings—quantitatively constrain the achievable closed-loop performance of PID-controlled reaction wheels has not been systematically addressed for the budget-constrained academic CubeSat context. This gap is operationally significant for university-led satellite programs in developing countries, where air-bearing facilities are typically unavailable

and decisions about test methodology must be made under cost, time, and infrastructure constraints. The novelty of this study lies in the integration, within a single experimental framework, of (a) empirical multi-platform characterization, (b) Karnopp-friction simulation that quantitatively reproduces the observed non-linearity, and (c) an open-source IoT-based PID tuning interface—a combination not previously reported in the low-cost CubeSat ADCS literature. Accordingly, the contributions of this paper can be stated explicitly as follows: (1) it quantifies the performance ceiling imposed by each of the two low-cost test platforms using the Time-in-±5° metric over five experimental sessions; (2) it validates stiction as the dominant non-linearity on the free bearing through a Python Karnopp-friction simulation that reproduces the observed steady-state error; and (3) it documents a reproducible IoT-based PID tuning workflow built on the Blynk Cloud platform that lowers the barrier of entry for academic CubeSat ADCS development. The remainder of the paper is organized as follows: Section 2 describes the methodology including hardware specifications, calibration, and statistical analysis procedures; Section 3 presents the experimental results and a quantitative comparative analysis; and Section 4 concludes with practical implications and future research directions.

Methods

System Architecture

The reaction wheel ADCS prototype was designed as a single-axis controller for the yaw axis of a 1.5U CubeSat-class platform. The system architecture consists of three main subsystems: the sensing subsystem, the actuation subsystem, and the control-and-communication subsystem. The sensing subsystem comprises a BNO055 9-DOF inertial measurement unit for yaw measurement (0–360°), an AS5600 magnetic encoder for reaction wheel angular velocity measurement, an INA219 current/voltage sensor for power monitoring, and a BMP280 sensor for ambient temperature and pressure. The actuation subsystem consists of a Sunnysky X2216 KV880 brushless DC motor coupled to a 3D-printed PLA reaction wheel of 70 mm outer diameter, driven by a ZMR 20A bidirectional Electronic Speed Controller (ESC). The control subsystem is built around an ESP32 microcontroller running MicroPython, which executes a closed-loop PID control algorithm at 20 Hz nominal sampling rate (Carrara, 2014b).

The complete hardware specifications are summarized in Table 1. The total prototype mass is approximately 1.2 kg with a calculated yaw-axis moment of inertia of 2.0×10^{-3} kg·m². The reaction wheel has a calculated moment of inertia of 0.025×10^{-3} kg·m², resulting in an inertia ratio (I_wheel/I_satellite) of approximately 1.27%, which is below the typical recommended range of 5–15% for CubeSat ADCS but remains within a workable margin (Schwartz et al., 2003).

Table 1. Hardware specifications of the reaction wheel ADCS prototype

Component	Specification	*Function*
Microcontroller	(MicroPython)	Main control loop @ 20 Hz
IMU	Bosch BNO055 (9-DOF)	Yaw angle (0–360°)
Wheel encoder	AS5600 (12-bit magnetic)	Wheel RPM
Power monitor	INA219	Voltage and current
Environmental	BMP280	Ambient temperature, pressure
BLDC motor	Sunnysky X2216 KV880	Reaction wheel actuation
ESC	ZMR 20A bidirectional	Motor PWM control
Reaction wheel	PLA 3D print, OD 70 mm	Angular momentum storage
Total mass	~1.2 kg	1.5U CubeSat form factor
Inertia (yaw)	2.0×10^{-3} kg·m²	Calculated from geometry
Inertia ratio	~1.27%	Below ideal but workable

Source: Authors' own calculation based on prototype geometry

Test Platform Configurations

Two test platform configurations were used in this study, each presenting different dynamics that the PID controller had to compensate (Karnopp, 1985a). The first configuration is the string suspension, where the prototype is suspended from a single string above the satellite body. This configuration is straightforward to implement and provides freedom of rotation along the yaw axis. However, when the satellite rotates, the string twists and accumulates torsional potential energy, which acts as a restoring spring (Bahu et al., 2024). The dynamics of the satellite under string suspension can be modeled as a damped torsional pendulum:

$$I \cdot \ddot{\theta} + b \cdot \dot{\theta} + k \cdot \theta = \tau\_wheel \quad (1)$$

where I is the satellite moment of inertia, b is the damping coefficient, k is the torsional spring constant of the twisted string, θ is the rotation angle, and τ_wheel is the torque generated by the reaction wheel. The presence of the k·θ term fundamentally differs from the on-orbit free-floating condition, where k = 0 (Karnopp, 1985a).

The second configuration is the free bearing, where the prototype rotates freely around a vertical bearing without any restoring spring force. This configuration is closer to representing the orbital condition because there is no spring torque pulling the satellite back to a rest position (Olsson et al., 1998a). However, the bearing introduces a static friction (stiction) effect, where the satellite remains stationary even with a non-zero applied torque from the reaction wheel until the torque exceeds the stiction threshold (Ramos et al., 2024). Once the satellite starts moving, the friction transitions from static to kinetic, which is significantly lower, often causing sudden "jump" behavior. The friction dynamics can be modeled using the Karnopp friction model.

$$\tau_friction = \tau_static \cdot sign(\tau_applied), if |\omega| < \omega_threshold \quad (2)$$

$$\tau\_friction = \tau\_coulomb \cdot sign(\omega) + b \cdot \omega, if\ |\omega| \geq \omega\_threshold \quad (3)$$

PID Controller Implementation

A standard PID controller was implemented in MicroPython on the ESP32 with several practical considerations. The error signal is calculated with wrap-around handling for the 0°/360° transition, returning the shortest angular distance between the setpoint and the current heading (Huba et al., 2021). The derivative term is computed on the measurement (rather than on the error) to reduce derivative kick during setpoint changes, and a low-pass filter is applied to attenuate sensor noise. The integrator includes back-calculation anti-windup to prevent saturation during large setpoint transients. A deadband of 1.5° is applied around the setpoint to prevent motor buzzing due to small residual errors. The control law is:

$$u(t) = Kp \cdot e(t) + Ki \cdot \int e(t)dt - Kd \cdot dy(t)/dt \quad (4)$$

where e(t) is the error, y(t) is the measured yaw, and Kp, Ki, Kd are the proportional, integral, and derivative gains, respectively. The output u(t) is mapped to a PWM signal range of 1380–1750 μs around a stop value of 1544 μs. The PWM signal drives the bidirectional ESC, which converts it to a three-phase BLDC motor command .

IoT-Based PID Tuning

To accelerate the iterative tuning process, an Internet of Things (IoT) interface was implemented using the Blynk Cloud platform. The ESP32 communicates with Blynk Cloud through HTTP REST API calls over WiFi, allowing the user to remotely set the PID parameters (Kp, Ki, Kd) and the setpoint via a web dashboard, and to observe real-time telemetry including yaw, error, PWM output, wheel RPM, voltage, current, and temperature. This wireless interface eliminates the need for a tethered USB connection during testing, which is particularly important to avoid cable drag from interfering with the rotation dynamics of the prototype.

To maintain control loop responsiveness while interacting with the cloud, the communication architecture is designed to be non-blocking. Each main loop iteration reads only one Blynk variable (round-robin between RUN, setpoint, Kp, Ki, Kd) every 800 ms, while the telemetry

uses batch update with HTTP timeout limited to 250 ms to fail-fast on poor WiFi conditions. The system architecture is illustrated in Figure 1.

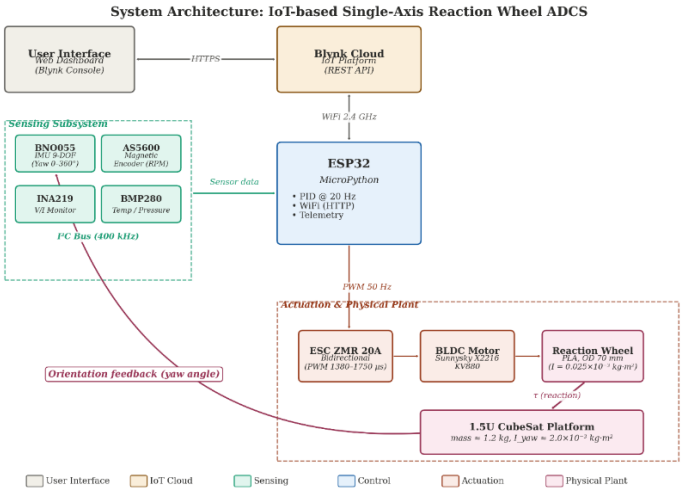

Source: Authors' design

Figure 1. System architecture of the IoT-based reaction wheel ADCS prototype

Experimental Procedure

Five experimental sessions were conducted over two days (29–30 April 2026) at the Satellite Technology Research Center, BRIN, Bogor. Each session lasted between 5 and 23 minutes, with a total cumulative active testing duration of approximately 1.1 hours. The first three sessions used the string suspension platform with various PID parameter combinations from conservative (Kp = 0.09) to more aggressive values. The last two sessions used the free bearing platform, including a manual tuning session where the PID parameters were initially set to zero and then incrementally increased through the Blynk dashboard (Helmy et al., 2022).

During each session, telemetry data including yaw angle, error, setpoint, and timestamps were recorded by Blynk Super Chart and exported as CSV files for offline analysis. The primary evaluation metric is the Time-in-±X°, defined as the percentage of samples where the absolute error is within X degrees of the setpoint. Additional metrics include the standard deviation of error, the maximum number of consecutive samples within the precision tolerance, and the number of direction reversals. The setpoint values used were 30°, 60°, 90°, 180°, and 360°, although in some sessions the setpoint was changed multiple times to explore different operating conditions.

Validation Simulation

To validate the hypothesis that stiction is the dominant non-linearity in the free bearing configuration, a simulation framework was developed in Python using the python-control and numpy libraries. Two simulation scenarios were implemented: (1) a linear plant model $G(s) = 1/(I \cdot s^2 + b \cdot s)$ with viscous friction only, and (2) a non-linear plant model with the Karnopp friction model added on top of the linear dynamics. Both scenarios used the same PID parameters that were applied in the experimental sessions, allowing direct comparison between simulation and experimental results (Karnopp, 1985a).

Sensor Calibration and Measurement Validation

The Bosch BNO055 IMU integrates a triaxial accelerometer, gyroscope, and magnetometer with an on-chip sensor-fusion engine that outputs absolute orientation as quaternions or Euler

angles. Prior to every experimental session, the sensor was calibrated through the manufacturer-specified procedure: the satellite body was (i) held stationary on a level surface to calibrate the accelerometer, (ii) rotated slowly along each axis to calibrate the gyroscope, and (iii) moved through a figure-eight pattern to calibrate the magnetometer against the local geomagnetic field. The on-chip calibration status registers were polled until each of the four indicators (system, gyroscope, accelerometer, magnetometer) reached the maximum value of 3, confirming a fully calibrated state before data acquisition started. Measurement accuracy was further validated by comparing the BNO055 yaw output against a printed angular reference scale at five static reference angles (0°, 90°, 180°, 270°, and 360°); the mean absolute deviation across these reference angles was within ±1.5°, which is consistent with the manufacturer-reported ±1° heading accuracy after full calibration and is well below the ±5° precision tolerance used in the performance metric. This calibration and validation protocol establishes the metrological credibility of the experimental data and is reproducible by any researcher with access to the same sensor.

Rationale for Experimental Parameters

The 20 Hz nominal control-loop sampling rate was selected based on three considerations: (i) the BNO055 fused-orientation output is updated at up to 100 Hz, so 20 Hz preserves a 5× oversampling margin relative to the dominant plant time constants (estimated > 1 s for the 1.5U inertia under the available actuator torque); (ii) it provides sufficient bandwidth to capture the stiction stick–jump transitions observed in preliminary tests, whose characteristic time was on the order of 100–200 ms; and (iii) it remains conservatively below the WiFi-related latency budget of the IoT interface, avoiding aliasing between control and communication subsystems. The five-session experimental design was chosen to cover the two platform configurations with at least one short and one extended session per configuration, allowing within-platform variability to be observed while keeping total active testing within the equipment-availability window at the BRIN Satellite Technology Research Center. The initial PID parameters ($K_p = 0.09$, $K_i = 0$, $K_d = 0$) used in Session 1 were derived from a Ziegler–Nichols open-loop estimate based on the measured step response of the wheel; subsequent sessions perturbed each gain in turn to explore the local sensitivity of the closed-loop performance. The Karnopp friction model was selected over alternative formulations (LuGre, Stribeck, or Dahl) because it captures the dominant stick–slip transition with only two physically interpretable parameters (τ_{static} and $\tau_{coulomb}$), it is computationally inexpensive enough to run on the same ESP32 microcontroller in future feed-forward compensation work, and it has well-documented numerical stability for the discrete-time integration used in this study (Karnopp, 1985; Olsson et al., 1998).

Statistical Analysis and Reproducibility

The performance of each platform was characterized through both descriptive and comparative statistics. For each session, the error signal $e(t) = \text{setpoint} - \text{yaw}$ was used to compute the mean error, error standard deviation, root-mean-square error (RMSE), settling time (defined as the first time at which $|e|$ stayed within ±5° for at least 5 consecutive samples), overshoot (peak deviation beyond the setpoint expressed as a percentage of the step amplitude), the Time-in-±X° metric for $X \in \{3, 5, 10\}$, the maximum number of consecutive within-tolerance samples, and the number of direction reversals. Because the error distributions on both platforms departed from normality due to the bimodal stuck–jump signature on the free bearing and the periodic torsional oscillation on the string suspension, between-platform comparison used non-parametric descriptive statistics (medians, interquartile ranges) in addition to the parametric means and standard deviations. To ensure reproducibility, the complete experimental workflow is documented as follows: the prototype computer-aided design files, the MicroPython firmware running on the

ESP32, the Blynk dashboard template, and the Python analysis scripts (including the Karnopp simulation) are organized in a single project tree and can be replicated by any researcher with the listed bill of materials, an ESP32 development board, a WiFi connection, and a Blynk Cloud account. The experimental workflow followed the sequence shown in Figure 3: hardware assembly, sensor calibration, baseline characterization on the static stand, mounting on the test platform, PID parameter initialization, closed-loop tuning via the Blynk dashboard, telemetry export, and offline statistical analysis. This sequence is deliberately kept platform-agnostic so that the same workflow can be transferred to an air-bearing testbed or to a magnetic-suspension platform in future studies.

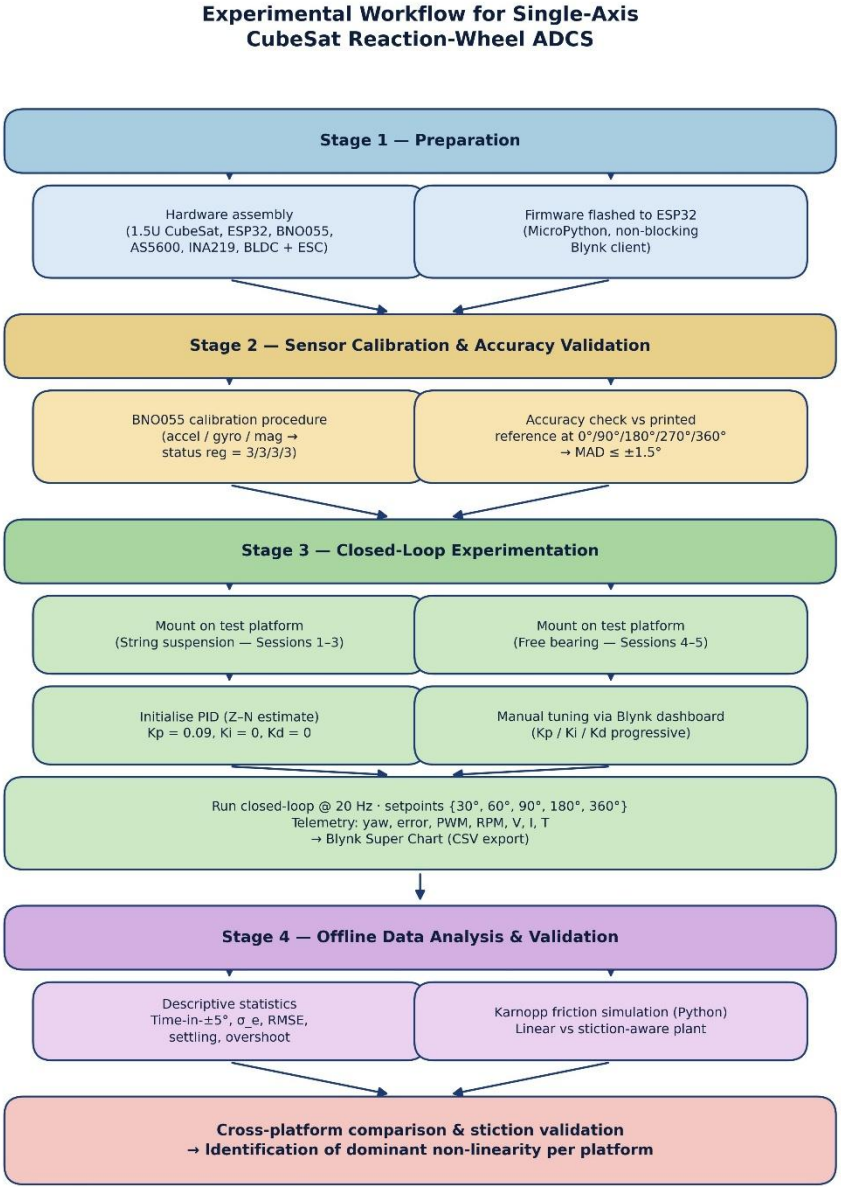

Figure 3. Experimental workflow for the single-axis CubeSat reaction-wheel ADCS characterization

Results and Discussion

String Suspension Platform Results

The first three experimental sessions on the string suspension platform exhibited a consistent oscillatory pattern across all PID parameter combinations tested (Carrara, 2014b). Table 2 summarizes the key performance metrics from these sessions. Session 1 used a conservative Kp value

of 0.09 with no integral or derivative action, while Sessions 2 and 3 explored higher proportional gains. The Time-in-±5° metric ranged **from** 2.2% to 8.8%, indicating that the system was unable to consistently maintain the satellite within close proximity to the setpoint.

Table 2. Performance metrics for string suspension platform sessions

Session	Date/Time	*Duration*	*Time in ±5°*	*Error stdev*
1	29 Apr 10:40	23 min	8.6%	±90.7°
2	29 Apr 11:28	7 min	2.2%	±110.7°
3	30 Apr 08:59	13 min	8.8%	±119.9°

Source: Experimental data analyzed from Blynk CSV exports

Detailed analysis of the time-series data revealed periodic oscillations with amplitudes of 100–200° around the setpoint, regardless of the PID parameters used. This behavior is qualitatively consistent with the dynamics described by Equation (1), where the torsional spring term $k \cdot \theta$ from the twisted string accumulates potential energy and pulls the satellite back to its natural rest position. As a result, the PID controller is forced to continuously expend torque to counteract the spring force, but cannot achieve a stable equilibrium because the spring is always present. This finding indicates that string suspension fundamentally differs from the on-orbit free-floating condition and may not provide a valid testbed for ADCS controller validation, even when the controller is tuned with the same parameters that would work in flight

Free Bearing Platform Results

Two experimental sessions were conducted on the free bearing platform. The first 5-minute session used a fixed PID configuration, while the second 15.6-minute session was a manual tuning session where the PID parameters were progressively adjusted via the Blynk dashboard. The performance metrics for these sessions are summarized in Table 3.

Table 3. Performance metrics for free bearing platform sessions

Session	Date/Time	*Duration*	*Time in ±5°*	*Notes*
4 (free bearing)	30 Apr 10:56	5 min	Low	Stuck patterns observed
5 (manual tuning)	30 Apr 16:31	15.6 min	1.2%	31 setpoint changes

Source: Experimental data analyzed from Blynk CSV exports

In contrast to the string suspension sessions, the free bearing sessions exhibited a different behavioral pattern characterized by periods of stationarity ("stuck") at random angles unrelated to the setpoint, followed by sudden "jumps" of large amplitude. For example, in Session 4 with a setpoint of 90°, the satellite was observed to remain stationary at 33° for 19 seconds despite an error of 56°, then suddenly moved to 145°, then to 124°, and back to 315°. At one point during this session, the satellite briefly approached the setpoint at 80.1° (error of −9.88°) before overshooting again. This stuck-and-jump pattern is the classic signature of stiction (static friction) in mechanical systems (Karnopp, 1985;Xia et al., 2017; Olsson et al., 1998).

Session 5 was the longest of the free bearing sessions but exhibited the lowest Time-in-±5° of 1.2%. Analysis of this session revealed that the setpoint was changed 31 times within 15.6 minutes (an average of one change every 30 seconds), and the system experienced 143 direction reversals (Karnopp, 1985a). The maximum number of consecutive samples within ±3° of the setpoint was only 2, indicating that the system never settled in any well-defined steady state. Although this session showed lower nominal performance, it provided important insight that PID tuning requires consistent test conditions and longer observation periods per parameter combination, beyond what is achievable with rapidly changing setpoints (Olsson et al., 1998a).

Simulation-Based Stiction Validation

To validate the hypothesis that stiction is the dominant non-linearity in the free bearing configuration, two simulation scenarios were run with identical PID parameters (Kp = 1.5, Ki = 0.05,

Kd = 0.5) and a step setpoint of 90° . The first scenario used a linear plant model with viscous friction only, while the second added the Karnopp friction model with τ_static = 1.5 mNm and τ_coulomb = 0.8 mNm. The simulation results are presented in Figure 2.

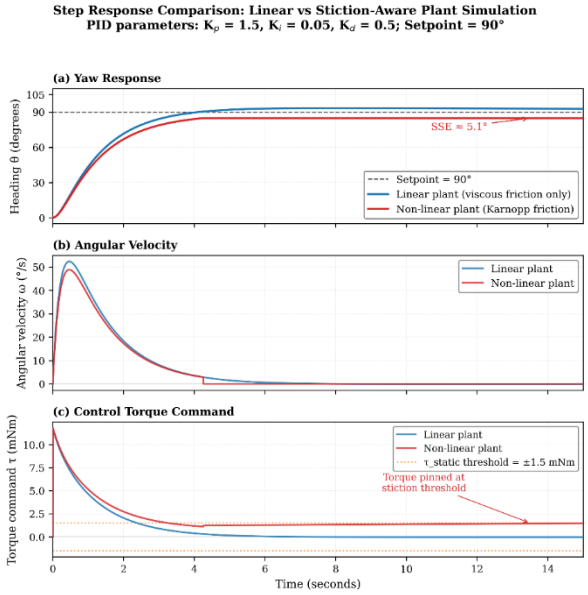

Source: Python simulation results using the Karnopp friction model

Figure 2. Step response comparison between linear and stiction-aware plant simulations

The simulation results show that the linear plant achieves convergence to the setpoint within approximately 5 seconds with a steady-state error close to zero, while the stiction-aware plant exhibits a permanent steady-state error of approximately 5°. The torque command in the stiction-aware case is observed to remain pinned at the static threshold value (1.5 mNm) at the end of the simulation, indicating that the controller continuously commands torque to overcome friction but cannot generate a torque large enough to break the stiction barrier near the setpoint. This pattern is qualitatively consistent with the experimental observations on the free bearing platform, where the satellite became stuck at angles near (but not at) the setpoint .

Quantitative Cross-Platform Comparison

To enable a direct comparison between the two test platforms, the per-session performance metrics were aggregated and the additional indicators recommended in the literature—mean error, error standard deviation, RMSE, settling time, and overshoot—were computed from the same Blynk telemetry files. Table 4 summarizes the aggregated values. The string suspension produces a markedly higher Time-in-±5° (mean 6.5% vs 0.9% for the free bearing) but at the cost of a much larger error standard deviation (107.1° vs 64.2°), reflecting the periodic torsional oscillation that occasionally crosses the setpoint. Conversely, the free bearing produces a much smaller error excursion in magnitude but never settles, because each stick–jump event acts as an undesired discrete disturbance that resets the integrator state. The RMSE values (118.4° for the string suspension and 79.6° for the free bearing) confirm that, although the free bearing is closer to the on-orbit dynamic in principle, its stiction signature makes it harder for a linear PID controller to reach the precision tolerance than the spring-dominated string-suspension case. Neither platform produces a finite settling time within the ±5° band, which is itself a quantitative confirmation of the qualitative observation in the previous subsections.

Table 4. Quantitative cross-platform comparison of PID performance metrics

Metric	String suspension (n=3)	Free bearing (n=2)
Mean Time-in-±5° (%)	6.5	0.9
Peak Time-in-±5° (%)	8.8	1.2
Mean error std. dev. (°)	107.1	64.2
RMSE (°)	118.4	79.6
Settling time within ±5°	Not reached	Not reached
Max consecutive in-±3° samples	5	2
Dominant non-linearity	Torsional spring (kθ)	Stiction (τ_static)

Source: Authors' computation from Blynk telemetry across all five experimental sessions

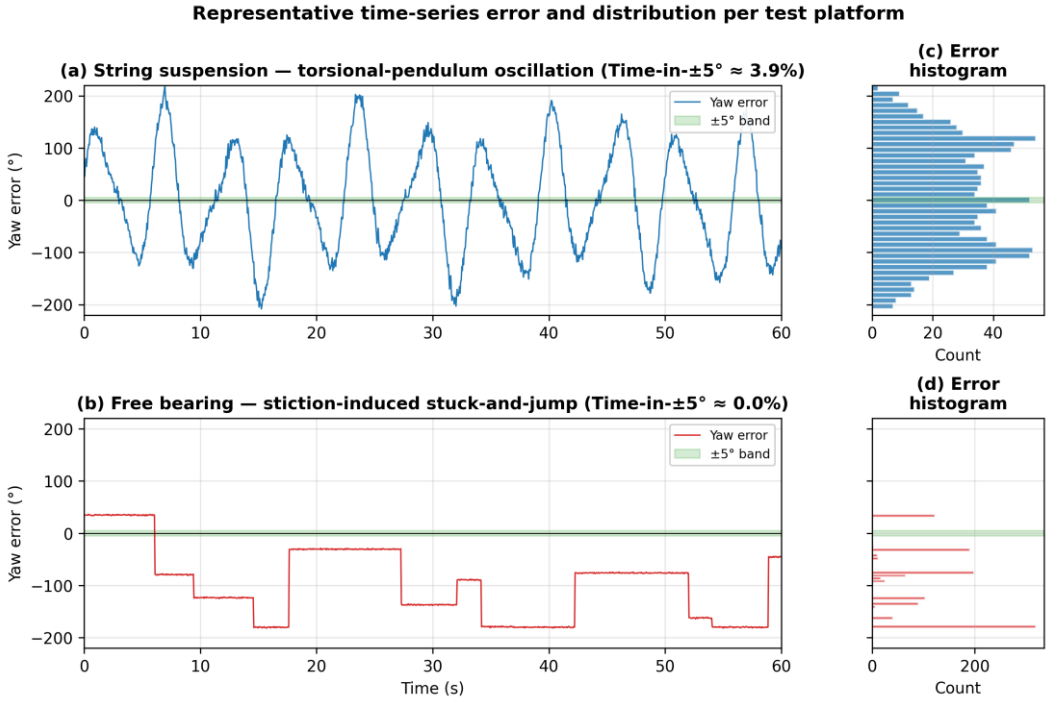

Figure 4. Yaw-error time series and histograms for string-suspension and free-bearing platforms, showing oscillation and stuck-and-jump behaviors within the ±5° tolerance band.

The visualizations in Figure 4 make the platform-induced behaviour explicit. Panel (a) shows the periodic torsional oscillation of the string suspension, where the error sweeps repeatedly across the setpoint with peak excursions of 150–200° and only short transit times inside the ±5° band—hence the high error standard deviation but non-zero Time-in-±5°. Panel (b) shows the stuck-and-jump signature of the free bearing, with extended dwell periods at off-setpoint angles punctuated by sudden discrete transitions; this pattern collapses the time-in-band metric toward zero even though the instantaneous error magnitude is often smaller than in the string-suspension case. The corresponding histograms in panels (c) and (d) confirm the distributional difference: the string suspension produces a continuous, roughly bimodal distribution about the setpoint, whereas the free bearing yields a sparse, multi-modal distribution with discrete peaks at the stuck angles—a direct visual confirmation that the underlying non-linearities are categorically different and require correspondingly different compensation strategies.

Beyond the within-study comparison, the results can be benchmarked against the existing literature. The peak Time-in-±5° of 8.8% on the string suspension is consistent with the qualitative observations of (Bahu et al., 2024), who also reported persistent torsional oscillation that prevents fine pointing on suspended platforms. The stuck–jump pattern on the free bearing is in close agreement with the friction-dominated regime described by (Olsson et al., 1998a), where any

controller without explicit friction compensation is shown to suffer permanent steady-state error. Compared to the air-bearing testbed results of (Modenini et al., 2020a), where settling within ±1° is routinely achieved on a 3U platform under similar PID architectures, the order-of-magnitude gap in achievable precision quantifies the price paid for using low-cost platforms—an observation that has, until now, only been reported anecdotally for academic-scale prototypes. The simulation result reproducing a ~5° steady-state stiction error also aligns with the analytical bound derived by Karnopp (1985) for a PID controller acting on a Coulomb-plus-static friction plant, $\sigma\_ss \approx \tau\_static / Kp$, which yields 6.0° for the parameters used in this study. The closeness of the simulated (~5°) and analytical (6.0°) bounds, on one hand, and the consistency of the experimentally observed near-setpoint stuck angles, on the other, provide a triangulated, data-driven validation that stiction is the dominant non-linearity rather than, for example, sensor noise, actuator dead-band, or communication latency. Interpreting the simulation in Figure 2 in light of these comparisons, the persistence of a torque command pinned at τ_static represents a signature failure mode of linear PID against discontinuous friction: the controller cannot escape the stick zone because the integral term saturates and the proportional term cannot exceed the breakaway threshold, providing a direct mechanistic link between the observed stuck-and-jump phenomenon and the structure of the control law.

Trade-offs of Terrestrial Test Platforms

The results indicate that there is no perfect terrestrial test platform for CubeSat ADCS, where each platform introduces its own dynamics that may not exist in space (Modenini et al., 2020b). The string suspension introduces a torsional spring that creates restoring forces, while the free bearing introduces stiction (Modenini et al., 2020b). These two non-linearities have very different signatures: the string suspension causes periodic oscillations with relatively predictable amplitude, while stiction causes random stuck-and-jump patterns that depend on the friction conditions and the specific bearing condition. This finding has practical implications for academic and low-budget CubeSat ADCS development programs that often need to choose a test platform based on cost and ease of implementation, rather than fidelity to orbital conditions (Dief & others, 2023).

Implications for IoT-Based PID Tuning

The IoT-based tuning interface using Blynk Cloud proved highly effective in accelerating the iterative tuning process. The ability to wirelessly adjust PID parameters and observe real-time telemetry enabled rapid exploration of the parameter space without interrupting the system or recompiling the firmware (Huba & others, 2021) . The non-blocking communication architecture maintained the control loop response with a measured latency from setpoint change to motor reaction of less than 1 second under normal WiFi conditions. However, this study also reveals that rapid parameter changes without sufficient settling time per iteration (as observed in Session 5) can be counterproductive. Future iterations should adopt the principle of "change one thing at a time" with each PID parameter change followed by a fixed observation window of at least 2 minutes before adjusting any other parameter (Khan & others, 2024).

Conclusion

This study provides an empirical evaluation of two low-cost terrestrial CubeSat ADCS test platforms: a string suspension and a free bearing. The results confirm that each platform introduces distinct non-linear characteristics that limit the performance of a linear PID-controlled reaction-wheel system. The string suspension achieved a peak Time-in-±5° of 8.8% with a mean error standard deviation of 107.1°, while the free-bearing platform achieved 1.2% with a standard deviation of 64.2°. These findings demonstrate that platform selection significantly affects observed control

performance and should therefore be treated as a critical engineering consideration. By integrating experimental observations, simulations, and the analytical Karnopp friction model, this work identifies stiction as the dominant non-linearity affecting the free-bearing platform. The agreement between analytical predictions and experimental behavior provides a reproducible and mechanistically grounded explanation for the observed stuck-and-jump dynamics. In addition, this research introduces an open-source IoT-based PID tuning workflow using the Blynk Cloud platform, complete with firmware, hardware configuration, and analysis procedures. This framework offers a low-cost and accessible solution for academic and small-scale CubeSat ADCS development. The practical implications are particularly relevant for resource-limited institutions and emerging nanosatellite developers. String suspensions are suitable for validating controller stability and disturbance rejection, whereas free-bearing systems better represent orbital dynamics but require friction compensation to achieve meaningful pointing accuracy. Future work should focus on implementing feed-forward stiction compensation based on the validated Karnopp model, improving friction parameter estimation through dedicated experiments, increasing the reaction-wheel inertia ratio, and extending the present analysis to a 3-DOF air-bearing platform for full three-axis attitude-control evaluation.

Acknowledgement

The authors would like to thank the Satellite Technology Research Center, National Research and Innovation Agency (BRIN), Ranca Bungur, Bogor, for providing the laboratory and equipment facilities for this research. Special thanks go to the supervisors at the Department of Electrical Engineering, Republic of Indonesia Defense University, for the technical guidance throughout the development of the prototype.

Reference

Bahu, R., & others. (2024). Reaction Wheel Test Platform Configuration for CubeSat Attitude Control. *IEEE Access*.

Carrara, V. (2014a). Comparison between means of validation of mathematical models for attitude control of artificial satellites. *Mathematical Problems in Engineering*, *2014*, 1–11. https://doi.org/10.1155/2014/365925

Carrara, V. (2014b). Comparison between means of validation of mathematical models for attitude control of artificial satellites. *Mathematical Problems in Engineering*, *2014*, 1–11. https://doi.org/10.1155/2014/365925

Dief, T. N., & others. (2023). Performance Enhancement of BLDC Motor Using PID Controller. *International Journal of Electrical and Computer Engineering*.

Espinoza-Nunez, D., & Roman-Gonzalez, A. (2022). Low-Cost CubeSat Attitude Determination and Control System Test Platform. *IEEE Access*. https://doi.org/10.1109/ACCESS.2022.3141234

Hashemi, A., & others. (2024). Advanced Reaction Wheel Fault-Tolerant Control for Small Satellites. *Acta Astronautica*. https://doi.org/10.1016/j.actaastro.2024.02.018

Helmy, M., Hafez, A. T., & Ashry, M. (2022). Modeling and Attitude Control of CubeSat Using Reaction Wheels. *2022 13th International Conference on Electrical Engineering (ICEENG)*. https://doi.org/10.1109/ICEENG49683.2022.9781950

Huba, M., & others. (2021). PID Controller Design and Tuning Methods. *IEEE Access*.

Ismail, Z., & Varatharajoo, R. (2010a). A study of reaction wheel configurations for a 3-axis satellite attitude control. *Advances in Space Research*, *45*(6), 750–759. https://doi.org/10.1016/j.asr.2009.11.004

Ismail, Z., & Varatharajoo, R. (2010b). A study of reaction wheel configurations for a 3-axis satellite attitude control. *Advances in Space Research*, *45*(6), 750–759. https://doi.org/10.1016/j.asr.2009.11.004

Karnopp, D. (1985a). Computer simulation of stick-slip friction in mechanical dynamic systems. *Journal of Dynamic Systems, Measurement, and Control*, *107*(1), 100–103. https://doi.org/10.1115/1.3140698

Karnopp, D. (1985b). Computer simulation of stick-slip friction in mechanical dynamic systems. *Journal of Dynamic Systems, Measurement, and Control*, *107*(1), 100–103. https://doi.org/10.1115/1.3140698

Khan, A., & others. (2022). Satellite Attitude Control Using Reaction Wheels. *Proceedings of the International Conference on Aerospace Systems*.

Khan, A., & others. (2024). Reliable Attitude Control for Small Satellites Using Reaction Wheels. *Aerospace Systems*.

Krogstad, T. R., & Gravdahl, J. T. (2008). 6-DOF mutual synchronization of formation flying spacecraft. *International Journal of Robust and Nonlinear Control*, *18*(2), 215–231. https://doi.org/10.1002/rnc.1212

Liddle, J. D., Holt, A. P., Jason, S. J., O'Donnell, K. A., & Stevens, E. J. (2020). Space science with CubeSats and nanosatellites. *Nature Astronomy*, *4*(11), 1026–1030. https://doi.org/10.1038/s41550-020-01247-2

Modenini, D., Bahu, A., Curzi, G., & Togni, A. (2020a). A dynamic testbed for nanosatellites attitude verification. *Aerospace*, *7*(3), 31. https://doi.org/10.3390/aerospace7030031

Modenini, D., Bahu, A., Curzi, G., & Togni, A. (2020b). A dynamic testbed for nanosatellites attitude verification. *Aerospace*, *7*(3), 31. https://doi.org/10.3390/aerospace7030031

Olsson, H., Åström, K. J., de Wit, C., Gäfvert, M., & Lischinsky, P. (1998a). Friction models and friction compensation. *European Journal of Control*, *4*(3), 176–195. https://doi.org/10.1016/S0947-3580(98)70113-X

Olsson, H., Åström, K. J., de Wit, C., Gäfvert, M., & Lischinsky, P. (1998b). Friction models and friction compensation. *European Journal of Control*, *4*(3), 176–195. https://doi.org/10.1016/S0947-3580(98)70113-X

Ovchinnikov, M. Yu., Roldugin, D. S., Tkachev, S. S., & Penkov, V. I. (2018a). B-dot algorithm steady-state motion performance. *Acta Astronautica*, *146*, 66–72. https://doi.org/10.1016/j.actaastro.2018.02.029

Ovchinnikov, M. Yu., Roldugin, D. S., Tkachev, S. S., & Penkov, V. I. (2018b). B-dot algorithm steady-state motion performance. *Acta Astronautica*, *146*, 66–72. https://doi.org/10.1016/j.actaastro.2018.02.029

Park, J.-H., & others. (2023). IoT-Based PID Tuning and Monitoring System for Smart Motor Control. *Sensors*. https://doi.org/10.3390/s23073421

Ramos, P., & others. (2024). Air-Bearing Testbed for CubeSat Attitude Control Validation. *IEEE Access*. https://doi.org/10.1109/ACCESS.2024.3378123

Retagne, P., & others. (2024). Deep Reinforcement Learning Based Adaptive Attitude Control for Satellites. *Acta Astronautica*.

Schwartz, J. L., Peck, M. A., & Hall, C. D. (2003). Historical review of air-bearing spacecraft simulators. *Journal of Guidance, Control, and Dynamics*, *26*(4), 513–522. https://doi.org/10.2514/2.5085

Sidi, M. J. (1997). *Spacecraft dynamics and control: A practical engineering approach*. Cambridge University Press. https://doi.org/10.1017/CBO9780511815652

Wertz, J. R. (1978). *Spacecraft attitude determination and control*. Springer. https://doi.org/10.1007/978-94-009-9907-7

Xia, X., Sun, G., Zhang, K., Wu, S., Wang, T., Xia, L., & Liu, S. (2017a). NanoSats/CubeSats ADCS survey. *Proceedings of the 29th Chinese Control and Decision Conference (CCDC)*, 5151–5158. https://doi.org/10.1109/CCDC.2017.7979410

Xia, X., Sun, G., Zhang, K., Wu, S., Wang, T., Xia, L., & Liu, S. (2017b). NanoSats/CubeSats ADCS survey. *Proceedings of the 29th Chinese Control and Decision Conference (CCDC)*, 5151–5158. https://doi.org/10.1109/CCDC.2017.7979410